energies

MDPI

Article

A Hybrid Tri-Stable Piezoelectric Energy Harvester with Asymmetric Potential Wells for Rotational Motion Energy Harvesting Enhancement

Dawei Man [1,2,*], Bangdong Jiang [1], Yu Zhang [1], Liping Tang [1,2], Qinghu Xu [1,2], Dong Chen [1,2] and Tingting Han [1,2]

[1] School of Civil Engineering, Anhui Jianzhu University, Hefei 230601, China; jiang12261x@163.com (B.J.); 19966516916@163.com (Y.Z.); tangliping2018@ahjzu.edu.cn (L.T.); qinghx@ahjzu.edu.cn (Q.X.); chenchenchu@163.com (D.C.); hantingting@ahjzu.edu.cn (T.H.)

[2] BIM Engineering Center of Anhui Province, Hefei 230601, China

* Correspondence: mandawei@ahjzu.edu.cn

Abstract: This paper proposes an asymmetric hybrid tri-stable piezoelectric energy harvester for rotational motion (RHTPEH). The device features an asymmetric tri-stable piezoelectric cantilever beam positioned at the edge of a rotating disk. This beam is uniquely configured with an asymmetric arrangement of magnets. Additionally, an elastic amplifier composed of a vertical and a rotating spring connects the beam's fixed end and the disk. This setup enhances both the rotational amplitude and vertical displacement of the beam during motion. A comprehensive dynamical model of the RHTPEH was developed using Lagrange's equations. This model facilitated an in-depth analysis of the system's behavior under various conditions, focusing on the influence of key parameters such as the asymmetry in the potential well, the stiffness ratio of the amplifier springs, the radius of the disk, and the disk's rotational speed on the nonlinear dynamic response of the system. The results show that the asymmetric hybrid tri-stable piezoelectric energy harvester makes it easier to harvest the vibration energy in rotational motion and has excellent power output performance compared with the symmetric tri-stable piezoelectric energy harvester. The output power magnitude of the system at higher rotational speeds increases as the radius of rotation expands, but when the rotational speed is low, the steady-state output power magnitude of the system is not sensitive to changes in the radius of rotation. Theoretical analysis and numerical simulations validate the effectiveness of the proposed asymmetric RHTPEH for energy harvesting in low-frequency rotating environments.

Keywords: piezoelectric energy harvester; rotational motion; asymmetric potential well; inter-well periodic motion; nonlinear dynamic response

Citation: Man, D.; Jiang, B.; Zhang, Y.; Tang, L.; Xu, Q.; Chen, D.; Han, T. A Hybrid Tri-Stable Piezoelectric Energy Harvester with Asymmetric Potential Wells for Rotational Motion Energy Harvesting Enhancement. *Energies* **2024**, *17*, 2134. https://doi.org/10.3390/en17092134

Academic Editor: Mahmoud Bourouis

Received: 1 April 2024
Revised: 23 April 2024
Accepted: 26 April 2024
Published: 30 April 2024

1. Introduction

Recent trends in the development of small-scale electronic devices have spurred significant research interest in the field of energy harvesting technologies. This innovative area has increasingly captured the attention of numerous scholars and researchers as a viable alternative to conventional batteries. Traditional batteries often suffer from short lifespans, significant maintenance challenges, and notable environmental pollution issues. Lately, the practice of harvesting energy from ambient vibrations has been extensively investigated. It is now considered a promising and viable technology for powering self-sufficient, maintenance-free wireless sensors in various applications within the internet of things (IoT). The piezoelectric energy harvester (PEH) is a novel type of electromechanical coupling device capable of harvesting and converting ambient vibration energy into electrical energy [1,2]. PEHs have been used in a wide range of applications including wireless sensor nodes, structural health monitoring devices, biomedical implanted devices, and aeronautical systems [3,4]. The versatility and utility of PEHs stem from their ability to utilize environmental vibrations as a power source, presenting a sustainable

alternative to traditional energy methods. Conventional PEHs are linear systems with high energy harvesting efficiency near resonance but a dramatic decline in efficiency away from resonance [5]. To address this limitation, extensive research has been undertaken to enhance the bandwidth of energy harvesting. Various studies have explored methods like tuning the resonant frequency of the harvesters to match the frequency of ambient vibrations [6–8]. Some studies have also presented multi-stable configurations, which have been shown to achieve high-efficiency energy conversion across a broader spectrum of frequencies [9–14]. Stanton et al. [15,16] derived a detailed mathematical model of the bistable energy harvester (BEH) and verified its heightened capabilities numerically and experimentally. Kim et al. [17,18] investigated a cantilever-beam-based magnetically coupled tri-stable energy harvester (TEH), and their results also demonstrated that the TEH is superior to the BEH for broadband energy harvesting at low levels of external excitation. Fang et al. [19] provided a critical review of the phenomenon of multistability in the context of energy harvesting. Their work outlines the primary challenges and difficulties associated with applying multi-stable systems practically, emphasizing the need for further research to overcome these hurdles and enhance the applicability of such technologies in real-world scenarios.

Parallel to the development of linear and nonlinear energy harvesters, there has been growing interest in devices capable of harnessing energy from rotational motion. Rotational piezoelectric energy harvesters (RPEHs) are gaining traction, particularly in applications involving rotating components such as wheels, bearings, gears, and wind turbine blades [20–26]. The advent of RPEHs introduces a novel approach to energy harvesting in rotational settings. Khameneifar et al. [27] designed a cantilever beam piezoelectric harvester that generates continuous vibration and harvests energy through the periodic excitation caused by the tip mass of the beam during rotational motion. Guan et al. [28] highlighted a novel nonlinear rotational vibration energy harvester that leverages the nonlinear magnetic forces produced by a set of magnets. Their findings, derived from both numerical simulations and experimental trials, suggest that this type of harvester shows enhanced performance in low-frequency rotational environments, surpassing the efficiency of traditional linear harvesters. Zhang et al. [29] proposed installing a BPEH that is connected to the wheel edge. This device is designed to convert the rotating energy of the wheel and the external exciting energy into electrical energy. The purpose of this electric energy is to power a vehicle's tire pressure monitor system. The process of harvesting energy from rotational motion has received much less research interest, and there are still a few obstacles to overcome, including limited bandwidth, low adaptation to rotational speed, poor dependability, and unsatisfactory efficiency. To address some of these challenges, Fu and Yeatman [30] developed a method that involves converting rotational motion into the vibrational motion of a piezoelectric beam. This approach, which uses frequency up-conversion via magnet plucking, has notably improved the output frequency and environmental adaptability of the harvesters. Machado et al. [31] presented an out-of-resonance RPEH that featured a variable stop in order to restrict the maximum displacement and enhance the amount of power that was harvested in the lower frequency range. Mei et al. [32] established a theoretical model of a magnetic tri-stable piezoelectric harvester based on rotational motion, analyzing the impact of different speeds and piezoelectric coupling coefficients on the system's energy harvesting efficiency.

Prior research has extensively explored the dynamics of rotational motion in energy harvesting devices, examining both linear and non-linear multi-stable configurations [33,34]. Among these, devices characterized by asymmetric potential energy stand out due to their lower potential deviations and inherently more unstable potential wells than their symmetric counterparts. This unique attribute has been theorized to significantly enhance the efficiency of energy harvesting [35]. Expanding on these foundational insights, our previous work introduced an innovative approach with the development of the hybrid tri-stable energy harvester (HTEH). This device ingeniously combines vertical and rotational elastic amplifiers to optimize energy conversion, which is especially effective when dealing

with low-level excitations. Such integration is designed to maximize the efficiency of energy harvesting by exploiting the natural dynamics of rotational motion. Despite the promising developments in asymmetric and hybrid configurations, there remains a noticeable lack of research focused on their performance specifically in rotational motion scenarios. To address this gap, our current study presents a detailed investigation into an asymmetric hybrid tri-stable piezoelectric energy harvester optimized for rotational motion (RHTPEH). This research aims to deepen the understanding of how these complex systems can be tailored to improve performance and efficiency in practical applications.

The structure of the paper is organized as follows: In Section 2, we derive the comprehensive equation for harmonic balancing solutions specifically for the asymmetric RHTPEH. This derivation is crucial for understanding the dynamic response mechanism of the device. In Section 3, both theoretical analysis and numerical simulations are employed to extensively explore the nonlinear dynamics characteristics of the asymmetric RHTPEH, providing detailed insights into its behavior under varying conditions. Finally, Section 4 presents the key findings and conclusions, summarizing the significant outcomes of the research and highlighting their implications in the field.

2. Modeling of the Asymmetric RHTPEH

Figure 1 shows an asymmetric RHTPEH installed on the rim of a disk with radius r. A pair of piezoelectric layers is adhered to both surfaces of the metal layer of a cantilever beam of length l. A tip magnet is fixed to the end of the beam, and the two external magnets are arranged vertically asymmetrically on the outer supports of the beam. d_h denotes the horizontal distance between the tip magnet and the two external magnets, and d_{v1} and d_{v2} denote the vertical distance between the tip magnet and the two external magnets, respectively. Let the intersection of the horizontal extension line leading from the tip magnet to the line between the external magnets be o, the midpoint of the line between the external magnets be o', and the distance between o and o' be d_0. The mass m_f at the fixed end of the beam is connected to the disk and the L-shaped frame through the rotation spring k_r and the vertical spring k_f, respectively. m_f, together with k_r and k_f, constitutes a new type of elastic amplifier that is capable of simultaneously increasing the rotational amplitude and vertical displacement of the cantilever beam in the rotational motion. The geometrical and material parameters of the system are shown in Table 1.

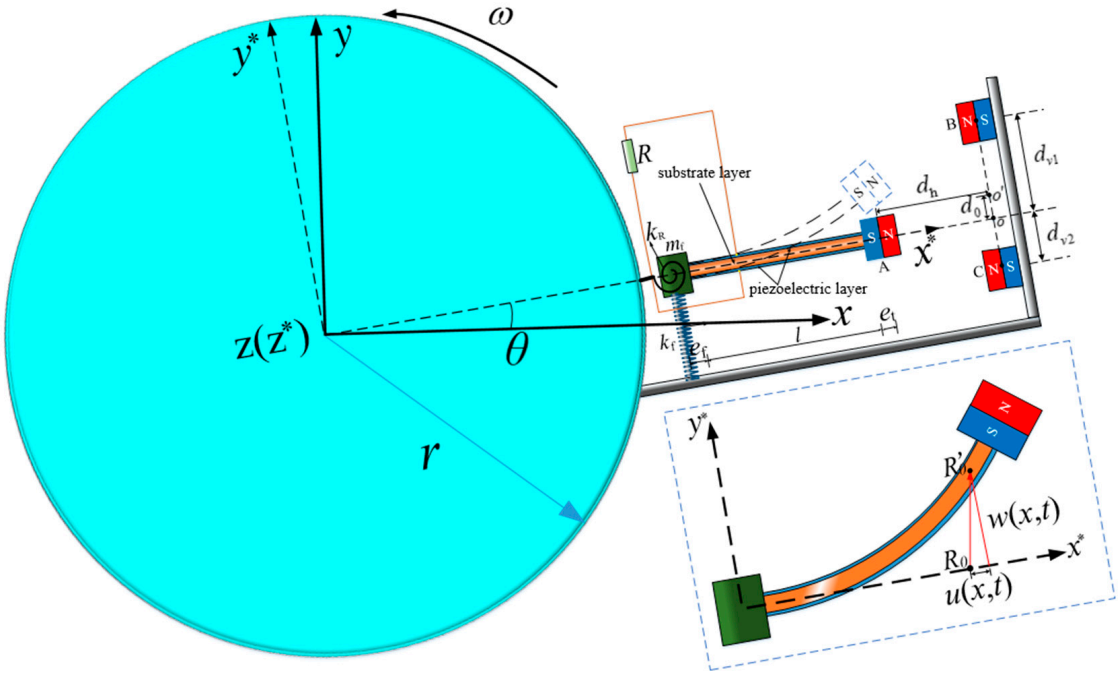

Figure 1. Configuration of the asymmetric RHTPEH.

Table 1. The geometric and material parameters of asymmetric RHTPEH.

Parameters	Symbol	Value
Mass of the tip magnet	m_t	15 g
Mass of the beam's fixed end	m_f	25 g
Length of the piezoelectric beam	l	90 mm
Width of the piezoelectric beam	b	22 mm
Thickness of the substrate layer	h_s	0.2 mm
Thickness of the piezoelectric layer	t_p	0.2 mm
Young's modulus of the substrate layer	Y_s	70 GPa
Density of the substrate layer	ρ_s	2700 kg/m^3
Density of the piezoelectric layer	ρ_p	7750 kg/m^3
Volume of the magnetic	V_A, V_B, V_C	1.0×10^{-6} m^{-3}
Damping ratio	ξ_1	0.01
Young's modulus of the piezoelectric layer	Y_p	60.98 GPa
Piezoelectric strain constant	d_{31}	-1.71×10^{-10} C/N
Stiffness of the rotation spring	k_r	50,000 N/m
Stiffness of the vertical spring	k_f	70,000 N/m
Piezoelectric dielectric constant	ε_{33}^s	-1.33×10^{-8} F/m

In Figure 1, xyz is the fixed coordinate system and $x^*y^*z^*$ is the rotating coordinate system. Assuming that R_0 is the position of the infinitesimal segment dx on the beam in the rotating coordinate system, $w(x,t)$ and $u(x,t)$ denote the transverse and axial displacements at x during the vibration of the beam, respectively. $\theta = \int_0^t \omega \mathrm{d}t$ denotes the angle of the x-axis with respect to the x^*-axis, where ω is the angular velocity of the disk rotation. The eccentricities of the tip magnet A and the mass m_f at the fixed end of the beam are e_t and e_f, respectively. The intrinsic relationships between the metal layer and the piezoelectric layer of the piezoelectric beam are given by Ref. [5]:

$$\left.\begin{aligned} N_1^S &= Y_S S_1^S \\ N_1^P &= Y_P (S_1^P - d_{31} E_3) \\ D_3 &= d_{31} N_1 + \varepsilon_{33}^T E_3 \end{aligned}\right\} \tag{1}$$

where quantities related to the metal layer are denoted by the superscript s, and quantities related to the piezoelectric layer are denoted by the subscript p; the x^* and y^* directions are denoted by the subscripts 1 and 3, respectively; and the symbols N, S, and Y stand for the stress, strain, and Young's modulus of the beam, respectively. D_3, d_{31}, and ε_{33}^T stand for the electrical displacement, the piezoelectric constant, and the dielectric constant, respectively. $E_3 = -V(t)/(2t_p)$, where $V(t)$ stands for voltage and t_p stands for the thickness of the piezoelectric layer. The expression for the relationship between displacement and strain is $S_1^s = S_1^p = -yw''$, where y represents the distance between the neutral axis of the beam and a point in its cross-section.

The Lagrange equation for the RHTPEH system is given by Ref. [32]:

$$L = T_k - U_e - U_g - U_c - U_d + W_e \tag{2}$$

where T_k, U_e, U_g, U_c, U_d, and W_e denote the kinetic energy, strain energy, gravitational potential energy, centripetal potential energy, amplifier elastic potential energy, and electrical energy of the system, respectively.

The kinetic energy of the system can be obtained from the geometric relationship in Figure 1 with the following equation:

$$\begin{aligned} T_{\mathrm{k}} &= \tfrac{1}{2}m_0\int_0^l\left\{\dot{\theta}^2 w(x,t)^2+\left[\dot{w}(x,t)+(x+r+u(x,t))\dot{\theta}\right]^2\right\}\mathrm{d}x \\ &+\tfrac{1}{2}m_{\mathrm{f}}\left\{\dot{\theta}^2 w(0,t)^2+\left[\dot{w}(0,t)-e_{\mathrm{f}}\dot{w}'(0,t)+(r+u(0,t))\dot{\theta}\right]^2\right\} \\ &+\tfrac{1}{2}m_{\mathrm{t}}\left\{\dot{\theta}^2 w(l,t)^2+\left[\dot{w}(l,t)+e_{\mathrm{t}}\dot{w}'(l,t)+(l+r+u(l,t))\dot{\theta}\right]^2\right\} \\ &+\tfrac{1}{2}J_{\mathrm{f}}\dot{w}'(0,t)^2+\tfrac{1}{2}J_{\mathrm{t}}\dot{w}'(l,t)^2 \end{aligned} \tag{3}$$

where m_{t} and m_{f} are the masses of the tip magnet and the mass at the fixed end of the beam, respectively. The equivalent mass per unit beam length is determined by $m_0 = 2\rho_{\mathrm{p}}t_{\mathrm{p}}b+\rho_{\mathrm{s}}h_{\mathrm{s}}b$, where ρ_{p} and ρ_{s} denote the densities of the piezoelectric layer and the metal substrate layer, respectively. J_{t} and J_{f} are their respective moment of inertia.

The strain energy U_{e} of the RHTPEH system can be expressed as

$$U_{\mathrm{e}} = \frac{1}{2}\int_0^l\left[YIw''(x,t)^2-\frac{1}{2}Y_{\mathrm{p}}bd_{31}\left(h_{\mathrm{s}}+t_{\mathrm{p}}\right)V(t)w''(x,t)\right]\mathrm{d}x \tag{4}$$

where $YI = \frac{2}{3}\left[Y_{\mathrm{s}}bh^3+Y_{\mathrm{p}}b\left(3h^2t_{\mathrm{p}}+3ht_{\mathrm{p}}{}^2+t_{\mathrm{p}}{}^3\right)\right]$ denotes the flexural stiffness of the beam.

The gravitational potential energy U_{g} of the RHTPEH system is

$$\begin{aligned} U_{\mathrm{g}} &= m_0g\int_0^l[(x+r)\sin\theta+w(x,t)\cos\theta]\mathrm{d}x \\ &+m_{\mathrm{f}}\mathrm{g}[r\sin\theta+w(0,t)\cos\theta] \\ &+m_{\mathrm{t}}\mathrm{g}[(l+r)\sin\theta+w(l,t)\cos\theta] \end{aligned} \tag{5}$$

The centripetal potential energy U_{c} of the RHTPEH system in rotational motion is

$$\begin{aligned} U_{\mathrm{c}} &= \tfrac{1}{2}\int_0^l\left[m_0r\dot{\theta}^2(l-x)+\tfrac{1}{2}m_0\dot{\theta}^2(l^2-x^2)\right. \\ &\left.+m_{\mathrm{f}}r\dot{\theta}^2+m_{\mathrm{t}}\dot{\theta}^2(l+r)\right]w'(x,t)^2\mathrm{d}x \end{aligned} \tag{6}$$

The elastic potential energy U_{d} of the elastic amplifier is

$$U_{\mathrm{d}} = \frac{1}{2}k_{\mathrm{r}}w'(0,t)^2+\frac{1}{2}k_{\mathrm{f}}w(0,t)^2 \tag{7}$$

The expression for the electrical energy W_{e} of the RHTPEH system can be expressed as

$$\begin{aligned} W_{\mathrm{e}} &= \tfrac{1}{4}Y_{\mathrm{p}}bd_{31}\left(h_{\mathrm{s}}+t_{\mathrm{p}}\right)V(t)\int_0^l w''(x,t)\mathrm{d}x \\ &+bl\varepsilon_{33}^{\mathrm{s}}\tfrac{V(t)^2}{4t_{\mathrm{p}}} \end{aligned} \tag{8}$$

where $\varepsilon_{33}^{\mathrm{s}} = \varepsilon_{33}^{\mathrm{T}}-d_{31}^2Y_{\mathrm{p}}$.

The transverse displacement $w(x,t)$ can be expressed as follows using Galerkin's method [16]:

$$w(x,t) = \sum_{r=1}^{n}\varphi_r(x)q_r(t) \tag{9}$$

where $\varphi_r(x)$ and $q_{\mathrm{r}}(t)$ are the r-th order mode shape function and generalized coordinates of the beam, respectively. The orthogonality condition for the vibration mode function is

$$\begin{aligned} &\int_0^l\varphi_s(x)m_0\varphi_r(x)\mathrm{d}x+\varphi_s(l)m_{\mathrm{t}}\varphi_r(l)+\varphi_s(l)m_{\mathrm{t}}e_{\mathrm{t}}\varphi'_r(l) \\ &+\varphi'_s(l)\left(J_{\mathrm{t}}+m_{\mathrm{t}}e_{\mathrm{t}}{}^2\right)\varphi'_r(l)+\varphi'_s(l)m_{\mathrm{t}}e_{\mathrm{t}}\varphi_r(l) \\ &+\varphi_s(0)m_{\mathrm{f}}\varphi_r(0)-\varphi_s(0)m_{\mathrm{f}}e_{\mathrm{f}}\varphi'_r(0) \\ &+\varphi'_s(0)\left(J_{\mathrm{f}}+m_{\mathrm{f}}e_{\mathrm{f}}{}^2\right)\varphi'_r(0)-\varphi'_s(0)m_{\mathrm{f}}e_{\mathrm{f}}\varphi_r(0)=\delta_{rs} \end{aligned} \tag{10}$$

$$\begin{aligned}&\int_0^l \frac{\mathrm{d}^2\varphi_s(x)}{\mathrm{d}x^2} YI \frac{\mathrm{d}^2\varphi_r(x)}{\mathrm{d}x^2}\mathrm{d}x + {\varphi'}_m(0)k_\mathrm{R}{\varphi'}_r(0)\\&+\varphi_m(0)k_\mathrm{f}\varphi_r(0) = {\omega_r}^2\delta_{rs}\end{aligned} \tag{11}$$

where δ_{rs} is the Kronecker function. The intrinsic frequency of the undamped vibration of the beam is $\omega_r = \lambda_r^2\sqrt{YI/(m_0 l^4)}$, and λ_r is the eigenvalue. λ_r and the mode function are calculated as described in the literature [36].

Based on the authors' previous work, the expression for the magnetic potential energy considering only the first-order modes and taking into account the eccentricity of the tip magnet can be expressed as

$$U_\mathrm{m} = k_0 + k_1 q_1 - \frac{1}{2}k_2{q_1}^2 + \frac{1}{3}k_3{q_1}^3 + \frac{1}{4}k_4{q_1}^4 + \frac{1}{5}k_5{q_1}^5 + \frac{1}{6}k_6{q_1}^6 + o({q_1}^7) \tag{12}$$

The expressions for the coefficients in Equation (12) are given in the literature [35].

Substituting Equation (9) into Equation (2) and then into the following Lagrange's variational equation yields

$$\begin{cases}\frac{\mathrm{d}}{\mathrm{d}t}\left(\frac{\partial L}{\partial \dot{q}_1}\right) - \frac{\partial L}{\partial q_1} = P(t)\\ \frac{\mathrm{d}}{\mathrm{d}t}\left(\frac{\partial L}{\partial \dot{V}}\right) - \frac{\partial L}{\partial V} = Q(t)\end{cases} \tag{13}$$

where $P(t) = -2\xi_1\omega_1\dot{\eta}_1(t)$ denotes the generalized dissipative force of the RHTPEH system, ω_1 is the first-order natural frequency, ξ_1 is the damping ratio of the system, and $Q(t)$ denotes the generalized output charge. Then the electromechanical coupling equations of the RHTPEH system can be obtained by using Equation (13) as shown:

$$\begin{aligned}&\ddot{q}_1 + 2\xi_1\omega_1\dot{q}_1 + {\omega_1}^2 q_1 + K_\mathrm{c}\dot{\theta}^2 q_1 + k_1 - k_2 q_1 + k_3{q_1}^2 + k_4{q_1}^3\\&+k_5{q_1}^4 + k_6{q_1}^5 + \chi\ddot{\theta} - \vartheta V = [-\Gamma g + F(t)]\cos\theta\end{aligned} \tag{14}$$

$$C_\mathrm{p}\dot{V} + \frac{V}{R} + \vartheta\dot{q} = 0 \tag{15}$$

In Equations (14) and (15), the expressions for the coefficients K_c, χ, ϑ, Γ, and C_p are given in the Appendix A, and F(t) denotes the external excitation induced by the action of the disk in contact with its surroundings.

Introducing dimensionless transformations such as $S(\tau) = q_1(t)/l$, $\tau = \omega_1 t$, and $\overline{V}(\tau) = VC_\mathrm{p}/(l\vartheta)$ into Equations (14) and (15) yields

$$\begin{aligned}&\ddot{S} + 2\xi_1\dot{S} + K_1 + (1 - K_2 + K_\mathrm{c}\omega^2)S + K_3S^2 + K_4S^3 + K_5S^4 + K_6S^5\\&+\overline{\chi}\ddot{\theta} - \Theta\overline{V} = \left[\overline{\Gamma}g + f(t)\right]\cos\omega\tau\end{aligned} \tag{16}$$

$$\dot{\overline{V}} + \alpha\overline{V} + \dot{S} = 0 \tag{17}$$

where $K_1 = k_1/{\omega_1}^2 l$, $\omega = \dot{\theta}/\omega_1$, $K_2 = k_2 l/{\omega_1}^2$, $K_3 = k_3 l^2/{\omega_1}^2$, $K_4 = k_4 l^2/{\omega_1}^2$, $K_5 = k_5 l^3/{\omega_1}^2$, $K_6 = k_6 l^2/{\omega_1}^2$, $\overline{\chi} = \chi/(l{\omega_1}^2)$, $\overline{\Gamma} = \Gamma/(l{\omega_1}^2)$, $f(t) = F(t)/(l{\omega_1}^2)$, $\Theta = \vartheta^2/(l{\omega_1}^2)$, and $\alpha = 1/(\omega_1 RC_p)$

This paper focuses on the rotational motion performance of RHTPEH at various constant rotational speeds without external excitation. Thus, when letting $\ddot{\theta} = 0$ and $f(t) = 0$, and considering the system's own gravity as the external excitation force F, Equation (16) can be rewritten as

$$\begin{aligned}&\ddot{S} + 2\xi_1\dot{S} + K_1 + (1 - K_2 + K_\mathrm{c}\omega^2)S + K_3S^2 + K_4S^3 + K_5S^4 + K_6S^5\\&-\Theta\overline{V} = F\cos\omega\tau\end{aligned} \tag{18}$$

3. Dynamical Analysis with Harmonic Balance Method

Here, we assume that the solutions of Equations (17) and (18) are:

$$\begin{cases} S(\tau) = A(\tau)\sin(\omega\tau) + B(\tau)\cos(\omega\tau) \\ \overline{V}(\tau) = C(\tau)\sin(\omega\tau) + D(\tau)\cos(\omega\tau) \end{cases} \tag{19}$$

Balancing the coefficients of the $\sin(\omega\tau)$ and $\cos(\omega\tau)$ terms after substituting Equation (19) into Equation (17), and eliminating all derivative terms with respect to time for steady state motion, yields

$$\begin{cases} C = \frac{\omega}{\omega^2+\alpha^2}(B\alpha - \omega A) \\ D = \frac{\omega}{\omega^2+\alpha^2}(-A\alpha - \omega B) \end{cases} \tag{20}$$

Then, substituting Equations (19) and (20) into Equation (18) and neglecting the higher order harmonic terms yields

$$\begin{aligned} &-\omega^2 A - 2\omega\xi B + (1 - K_2 + K_c\omega^2)A \\ &+\tfrac{3K_4}{4}(A^3 + AB^2) + \tfrac{5K_6}{8}(A^5 + 2A^3B^2 + AB^4) \\ &-\tfrac{\Theta\omega}{\omega^2+\alpha^2}\alpha B + \tfrac{\Theta\omega^2}{\omega^2+\alpha^2}A = 0 \end{aligned} \tag{21}$$

$$\begin{aligned} &-\omega^2 B + 2\omega\xi A + (1 - K_2 + K_c\omega^2)B \\ &+\tfrac{3K_4}{4}(A^2B + B^3) + \tfrac{5K_6}{8}(A^4B + 2A^2B^3 + B^5) \\ &+\tfrac{\Theta\omega}{\omega^2+\alpha^2}\alpha A + \tfrac{\Theta\omega^2}{\omega^2+\alpha^2}B = F \end{aligned} \tag{22}$$

Let the displacement amplitude of the steady state motion of the RHTPEH system be $a = \sqrt{A^2 + B^2}$ and the voltage amplitude be $u = \sqrt{C^2 + D^2}$. Squaring both sides of Equations (21) and (22) and adding them together gives

$$\begin{aligned} &a^2\left[-\omega^2 + \left(1 - K_2 + K_c\omega^2\right) + \tfrac{3K_4}{4}a^2 + \tfrac{5K_6}{8}a^4\right. \\ &\left.+\tfrac{\Theta\omega^2}{\omega^2+\alpha^2}\right]^2 + a^2\left[2\omega\xi_1 + \tfrac{\Theta\omega}{\omega^2+\alpha^2}\alpha\right]^2 = F^2 \end{aligned} \tag{23}$$

Thus, the steady-state displacement amplitude of the system in rotational motion can be derived from Equation (23), and the steady-state output voltage amplitude can be expressed as

$$u = \frac{\omega}{\sqrt{\omega^2 + \alpha^2}}a \tag{24}$$

4. Dynamic Performance Analysis

In the first part of this section, we explore the impacts of various parameters on the steady-state response of the asymmetric RHTPEH system. This analysis is based on the analytical solution obtained through the harmonic balance method. Critical parameters under investigation include the disk's rotation radius and speed, as well as the asymmetric arrangement and magnetization of the magnet. The validity of the analytical model is confirmed through swept-speed simulations. In the second part, the captive energy performance of the asymmetric RHTPEH in the time domain is numerically simulated by MATLABR2021b software.

When $d_0 = 0$, the two external magnets are symmetrically arranged, and the potential well of the system's tri-stable potential energy function is symmetric. When $d_0 \neq 0$, the two external magnets are arranged asymmetrically, and the potential well of the system's tri-stable potential energy function is in an asymmetric state. The influence of the asymmetric distribution characteristics of the potential well of the asymmetric HTPEH system on its steady state response in rotational motion is investigated with the system parameters of m_t = 15 g, m_f = 25 g, r = 0.3 m, and d_h = 14 mm. The steady-state displacement and output voltage response amplitude of the asymmetric RHTPEH, along with the rotational speed of

the disk under different d_0, are shown in Figure 2. It can be seen from Figure 2 that with the increase in d_0, the steady-state displacement and output voltage response amplitude of the system are substantially increased, indicating that the asymmetric RHTPEH is more advantageous in terms of harvesting energy compared to the symmetric RHTPEH. As shown in Figure 3, when d_0 remains the same, increasing d_h leads to an increase in the steady-state displacement and output voltage amplitude of the asymmetric RHTPEH, but the rotational speed range that generates the inter-well motion decreases accordingly. In addition, as d_h increases, the steady-state displacement and output voltage amplitude of the asymmetric RHTPEH increase more significantly compared to the symmetric RHTPEH. Figures 2 and 3 also show the swept-speed numerical simulation of the steady-state output voltage amplitude of the system at different speeds, and the simulation results are basically in agreement with the analytical solution derived using the harmonic balance method.

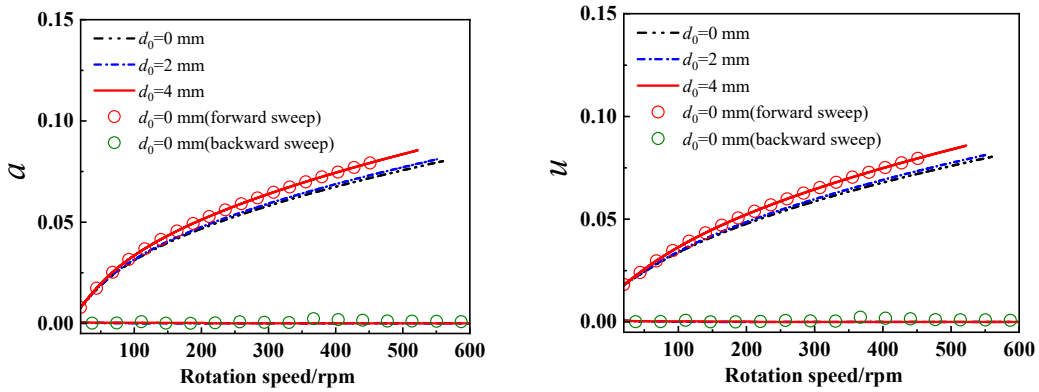

Figure 2. (**a**) Displacement response amplitude and (**b**) output voltage response amplitude of the asymmetric RHTPEH versus the rotational speed for different d_0 when d_h = 14 mm.

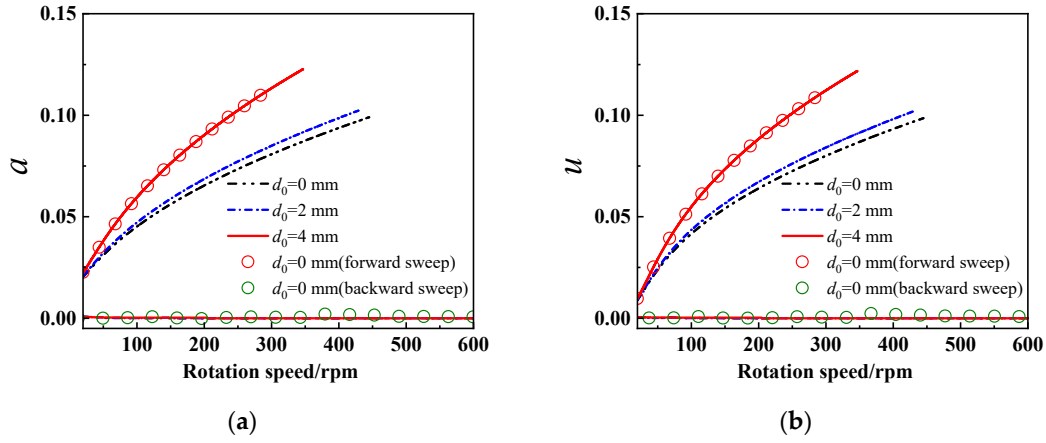

Figure 3. (**a**) Displacement response amplitude and (**b**) output voltage response amplitude of the asymmetric RHTPEH versus the rotational speed for different d_0 when d_h = 16 mm.

We define $\overline{k}$ as the stiffness ratio of the rotation and vertical springs. Figure 4 demonstrates the influence of the spring stiffness ratio $\overline{k}$ on the steady-state response of the asymmetric RHTPEH system in rotational motion with the system parameters of m_t = 15 g, m_f = 25 g, r = 0.3 m, d_0 = 4 mm, and d_h = 14 mm. Figure 4 shows that the range of rotational speeds for inter-well motion in the asymmetric RHTPEH system noticeably widens as the value of $\overline{k}$ increases, while the peak values of steady-state displacement and output voltage show a slight increase. When $\overline{k}$ stays the same as d_h increases, it can be seen from Figure 5 that the peak values of the steady-state displacements and output voltages of the

asymmetric RHTPEH system increase, while the rotational speed range that causes the system to produce inter-well motions decreases.

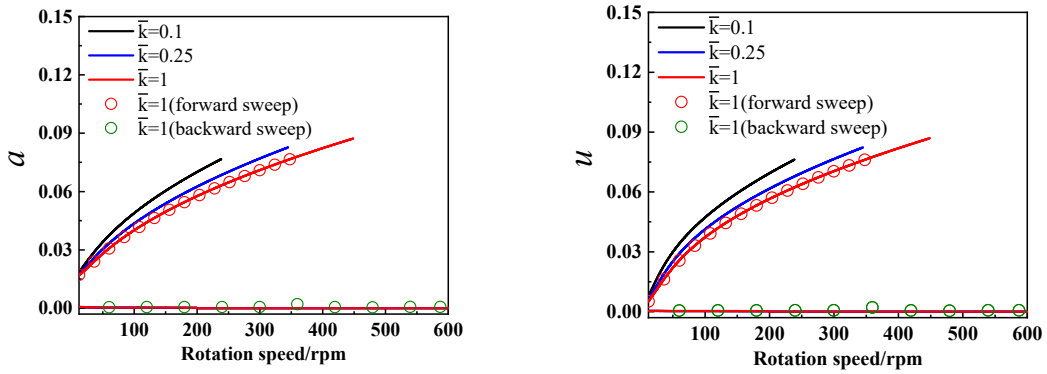

Figure 4. (**a**) Displacement response amplitude and (**b**) output voltage response amplitude of the asymmetric RHTPEH versus the rotational speed for different $\bar{k}$ when d_h = 14 mm.

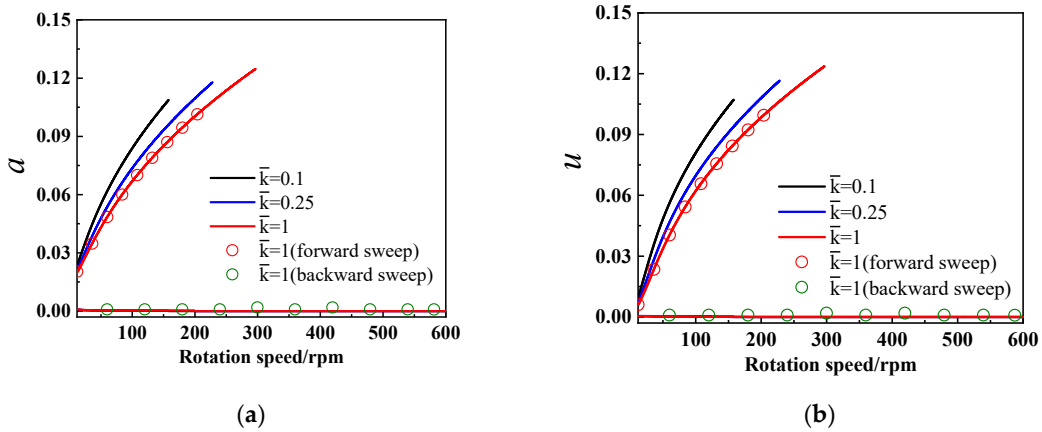

Figure 5. (**a**) Displacement response amplitude and (**b**) output voltage response amplitude of the asymmetric RHTPEH versus the rotational speed for different $\bar{k}$ when d_h = 16 mm.

The three-dimensional phase space diagrams of asymmetric RHTPEH (d_0 = 4 mm) and symmetric RHTPEH (d_0 = 0) at rotation speeds of 100 rpm, 200 rpm, 300 rpm, 400 rpm, and 450 rpm are shown in Figures 6–10, respectively. It can be seen from Figure 6 that when the rotational speed is 100 rpm, the symmetric RHTPEH (d_0 = 0) system can only oscillate slightly in the middle intra-well, producing a very small output voltage, while the asymmetric RHTPEH (d_0 = 4 mm) system undergoes chaotic motion, producing a large but unstable output voltage. As shown in Figure 7, increasing the rotation speed to 200 rpm causes the asymmetric RHTPEH (d_0 = 4 mm) to enter into the inter-well periodic motion after experiencing a brief chaotic motion, generating a large, stabilized output voltage, whereas the asymmetric RHTPEH (d_0 = 4 mm) falls back into the intra-well after a momentary chaotic motion for a small amplitude of oscillation. From Figures 8 and 9, it can be seen that when the rotation speed continues to increase to 300 rpm, both the symmetric RHTPEH (d_0 = 4 mm) and the symmetric RHTPEH (d_0 = 0) enter into periodic inter-well motion, but the output voltage produced by the asymmetric RHTPEH (d_0 = 4 mm) is higher, whereas the output voltages produced by both are close to each other when the rotation speed is 400 rpm. Finally, as shown in Figure 10, when the rotation speed is increased to 450 rpm, the symmetric RHTPEH (d_0 = 0 mm) can still break through the potential well bound into periodic inter-well motion, while the symmetric RHTPEH (d_0 = 4 mm) can only perform chaotic motion. From the above, it can be seen that the asymmetric RHTPEH is more suitable for energy harvesting at low rotation speeds.

The steady-state displacement and output power amplitude of the asymmetric RHTPEH, as well as the steady-state versus rotation radius and rotation speed, when d_h = 15 mm and d_0 = 4 mm are shown in Figures 11 and 12. As can be seen in Figures 11 and 12, when the rotational speed is lower than 100 rpm, the change in the radius of rotation has less effect on the steady-state displacement magnitude and steady-state output voltage magnitude of the system. However, once the rotational speed exceeds 100 rpm, the steady-state displacement magnitude and steady-state output power magnitude of the system will increase as the rotation radius increases. It is worth noting that the range of rotational speeds at which the asymmetric RHTPEH produces inter-well motion decreases when the radius of rotation increases during this phase. In addition, the tendency of the inter-well motion rotational speed range to decrease gradually slows down as the rotation radius increases. Although increasing the radius of rotation leads to a decrease in the rotational speed range of the inter-well motion generated by the asymmetric RHTPEH, the peak value of the output power increases. Therefore, according to the factors involved in actual application, such as the installation position and size of the energy harvester, as well as the specific application, we need to set an appropriate rotation radius in order to achieve the optimal energy harvesting efficiency of the asymmetric RHTPEH.

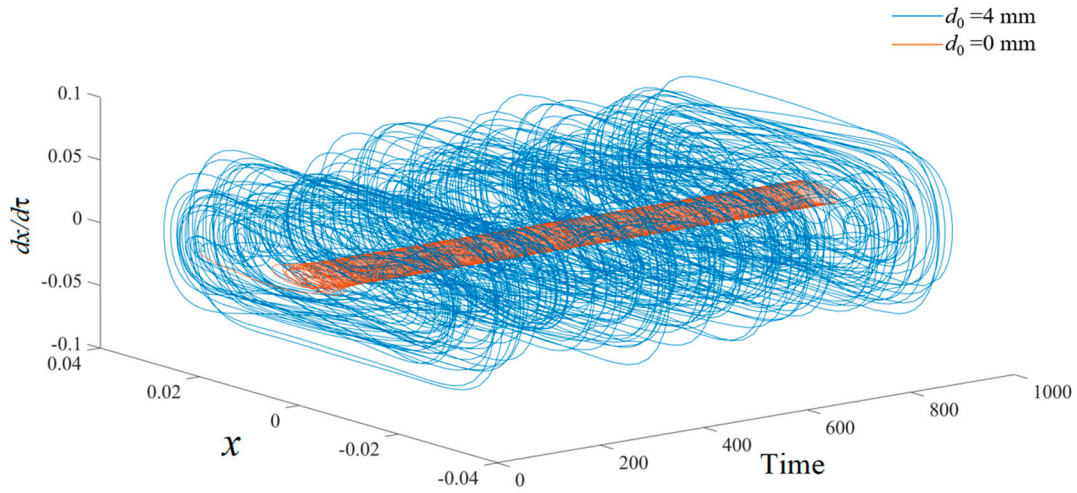

Figure 6. Three−dimensional phase space diagram for different d_0 when rotation speed is 100 rpm.

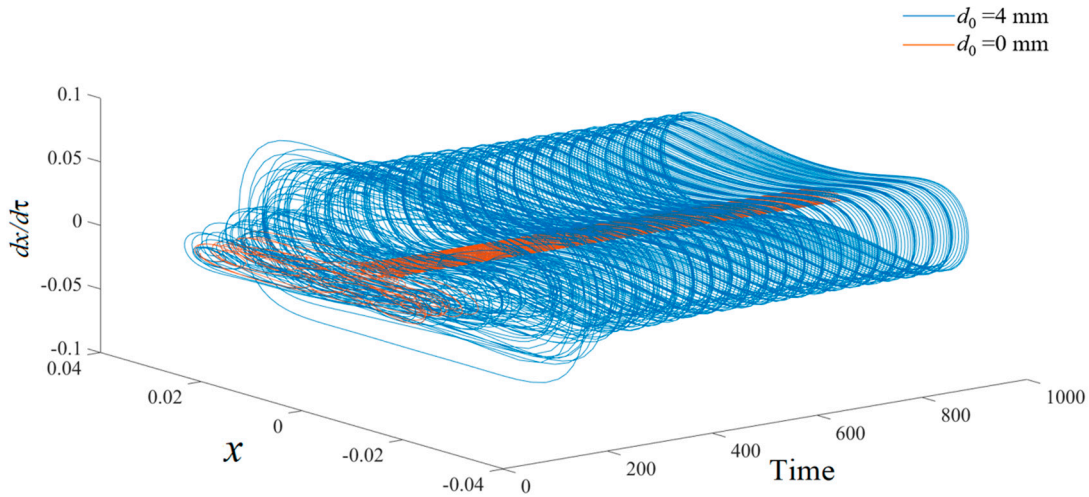

Figure 7. Three−dimensional phase space diagram for different d_0 when rotation speed is 200 rpm.

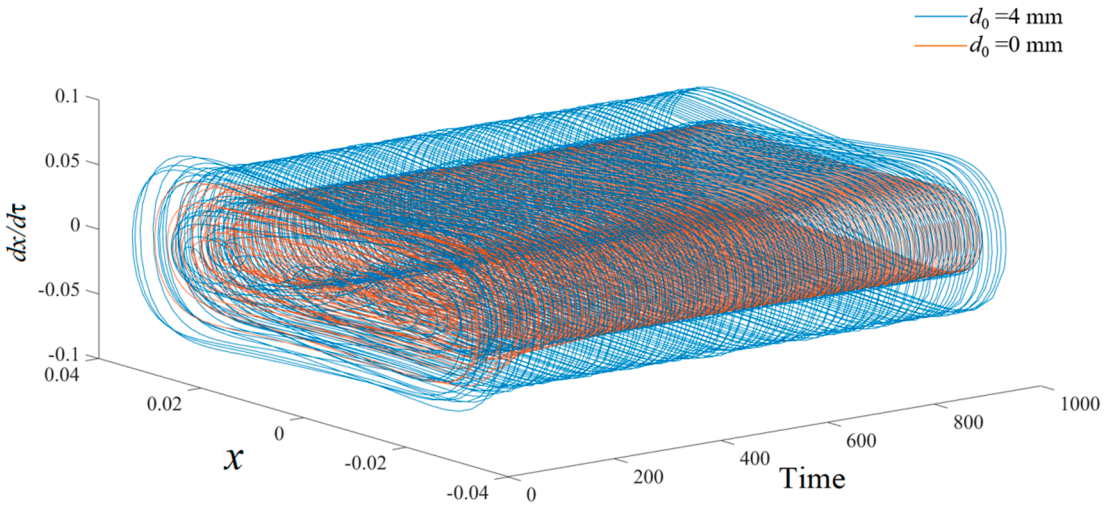

Figure 8. Three−dimensional phase space diagram for different d_0 when rotation speed is 300 rpm.

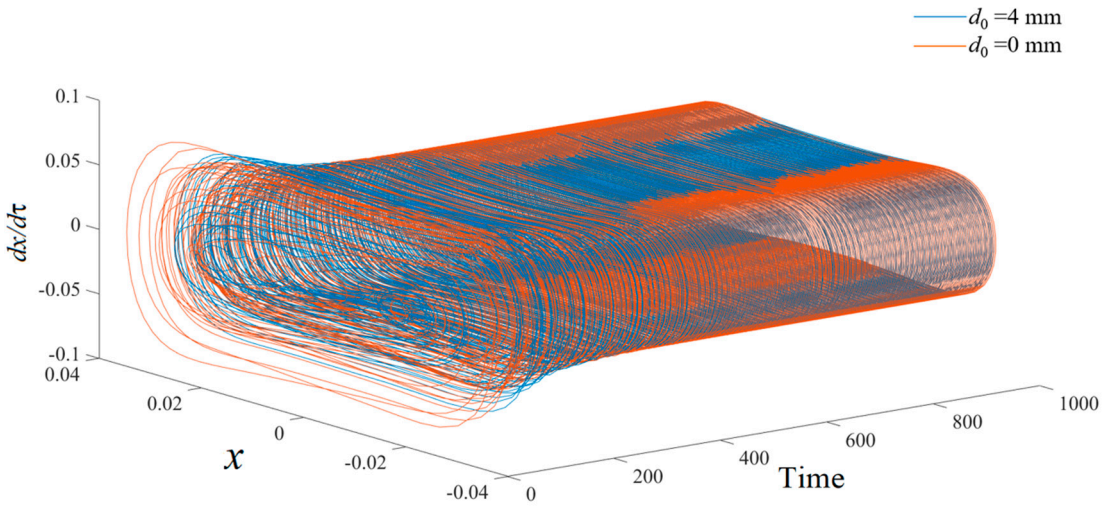

Figure 9. Three−dimensional phase space diagram for different d_0 when rotation speed is 400 rpm.

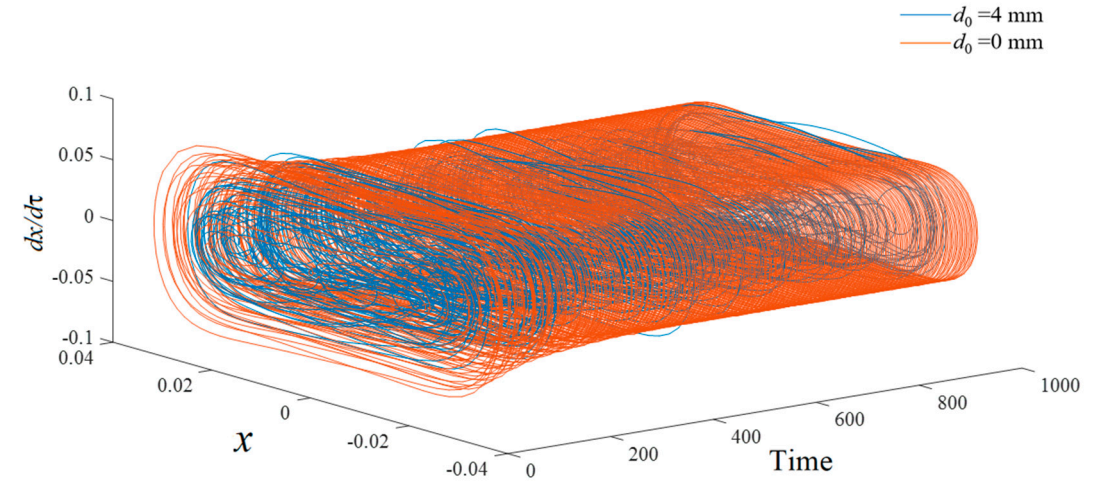

Figure 10. Three−dimensional phase space diagram for different d_0 when rotation speed is 450 rpm.

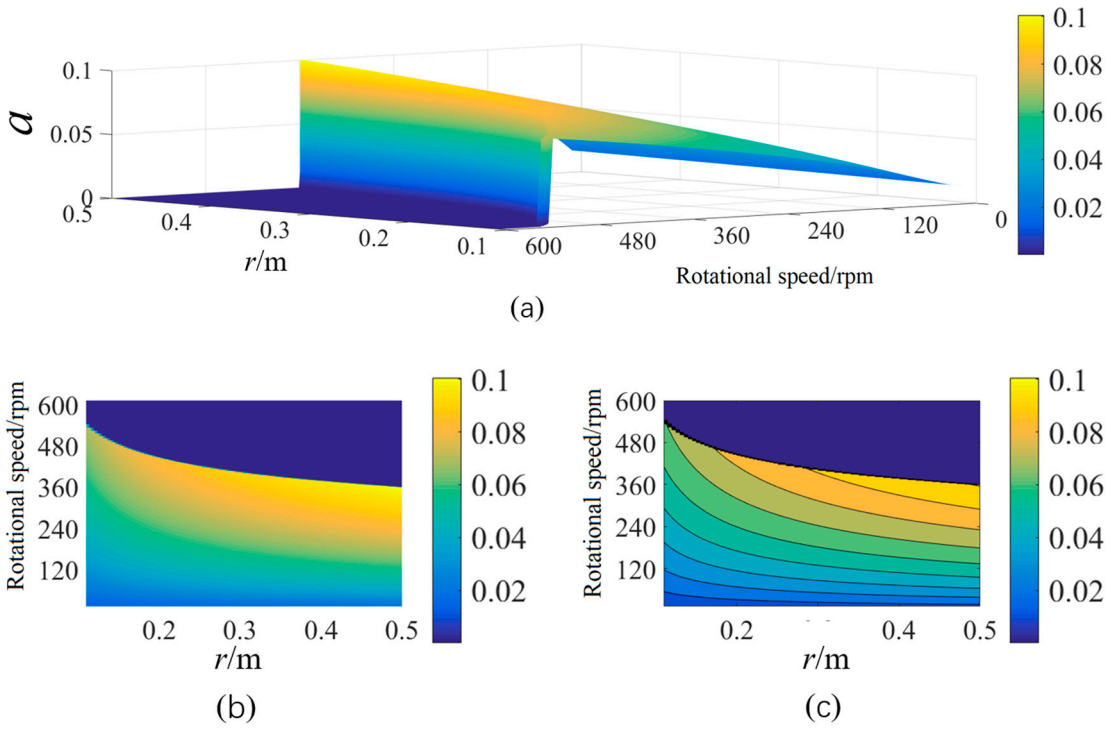

Figure 11. Displacement versus the rotational radius and the rotational speed: (**a**) 3D view; (**b**) vertical view; (**c**) contour of displacement.

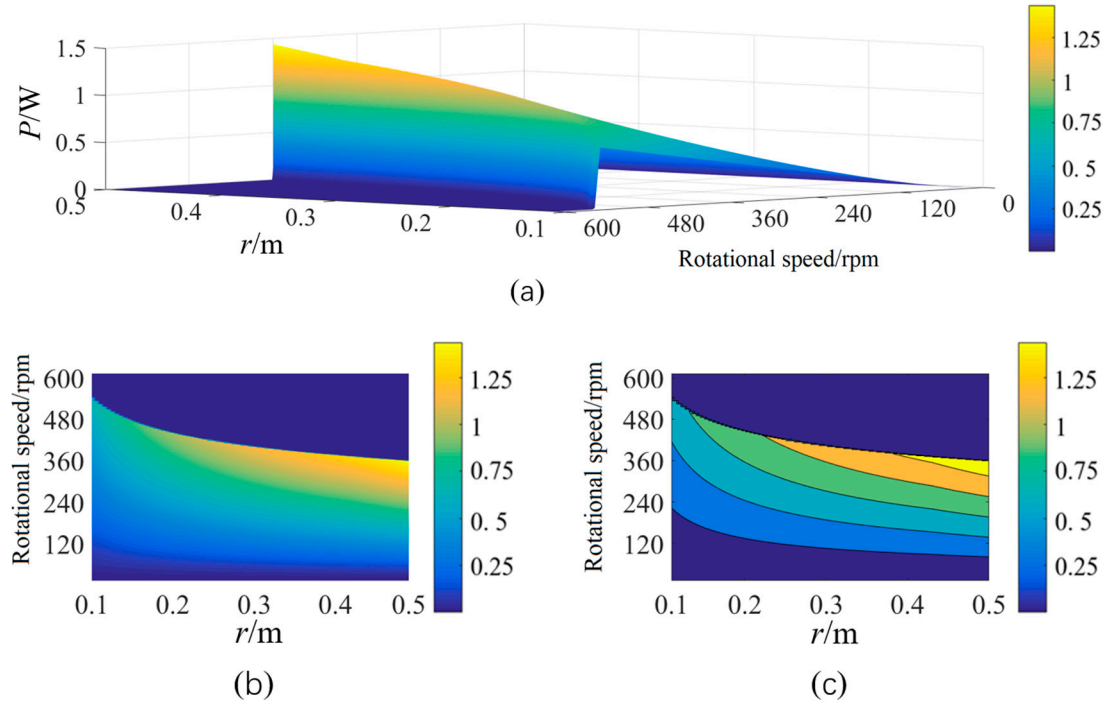

Figure 12. Output power versus the rotational radius and the rotational speed: (**a**) 3D view; (**b**) vertical view; (**c**) contour of output power.

5. Conclusions

In this paper, we propose an asymmetric hybrid tri-stable piezoelectric energy harvester in rotational motion (RHTPEH), derive a computational model of the system through the Lagrange's variational principle, and verify the effects of parameters such as the asymmetric state of the potential wells, the spring stiffness ratio, the rotational radius, and the

rotational speed on the nonlinear dynamic response of the system both theoretically and numerically simulated, and the main conclusions drawn are as follows.

(1) Compared to the symmetric RHTPEH, the asymmetric state of the potential well of the asymmetric RHTPEH results in a significant increase in its steady-state output voltage magnitude in rotational motion.
(2) Increasing the stiffness ratio of the rotation and vertical spring can significantly increase the range of rotational speeds for inter-well motion in the asymmetric RHTPEH system, while the peak values of steady-state displacement and output voltage only show a slight increase.
(3) The steady-state output voltage magnitude of the asymmetric RHTPEH is very slightly affected by the radius of rotation at lower rotational speeds, whereas when the rotational speed exceeds 100 rpm, the steady-state output voltage magnitude of the asymmetric RHTPEH increases with the radius of rotation, but the range of rotational speeds generating the inter-well motion decreases with it.
(4) The asymmetric RHTPEH is more likely to break through the potential barrier confinement into substantial periodic inter-well motion at lower rotational speeds (300 rpm), whereas the symmetric RHTPEH system is more likely to produce periodic inter-well motion at higher rotational speeds than 450 rpm.

In summary, the RHTPEH demonstrates significant potential for enhancing energy harvesting during rotational motion. The theoretical model outlined demonstrates its efficacy in predicting the dynamic behavior of the harvester in rotational motion. Optimizing the system's parameters is crucial for harnessing the full potential of this application.

Author Contributions: Conceptualization, D.M. and L.T.; Software, B.J. and Y.Z.; Validation, D.C.; Formal analysis, Q.X.; Data curation, D.M. and T.H. All authors have read and agreed to the published version of the manuscript.

Funding: This research was funded by the Anhui Provincial University Provincial Natural Science Research Project Key Project (2022AH050240), the Doctoral Startup Foundation of Anhui Jianzhu University (2020QDZ07), the Scientific Research Project of Anhui Education Department Key Project (KJ2021JD01), the Anhui Provincial Natural Science Foundation (2108085MA28), the Mechanical Properties Research of FRP Connectors in Fabricated Concrete Sandwich Insulation Wall Panels after Fire (KJ2021A0608), and the Anhui Provincial Course Ideological and Political Demonstration Course (2022kcsz060).

Data Availability Statement: The original contributions presented in the study are included in the article, further inquiries can be directed to the corresponding authors.

Conflicts of Interest: The authors declare no conflict of interest.

Appendix A

$$K_c = m_0\left\{r\int_0^l (l-x)\varphi_1'(x)^2\mathrm{d}x + \tfrac{1}{2}\int_0^l (l^2-x^2)\varphi_1'(x)^2\mathrm{d}x - \int_0^l \varphi_1(x)^2\mathrm{d}x\right\}$$
$$+m_f\left[r\int_0^l \varphi_1'(x)^2\mathrm{d}x - \varphi_1(0)^2\right] + m_t\left[(l+r)\int_0^l \varphi_1'(x)^2\mathrm{d}x - \varphi_1(l)^2\right]$$

$$\chi = m_0\int_0^l (x+r)\varphi_1(x)\mathrm{d}x + m_f r\varphi_1(0) + m_t(l+r)\varphi_1(l)$$
$$-m_f e_f\varphi_1'(0) + m_t e_t(l+r)\varphi_1'(l)$$

$$\vartheta = Y_p b d_{31}\left(h + \frac{t_p}{2}\right)\int_0^l \varphi_1''(x)^2\mathrm{d}x$$

$$\Gamma = m_0\int_0^l \varphi_1(x)\mathrm{d}x + m_t\varphi_1(l) + m_f\varphi_1(0)$$

$$C_p = \frac{bl\varepsilon_{33}^S}{2t_p}$$

References

1. Wei, C.; Jing, X. A comprehensive review on vibration energy harvesting: Modeling and realization. *Renew. Sustain. Energy Rev.* **2017**, *74*, 1–18. [CrossRef]
2. Moshen, S.; Henry, S.A.; Steven, A.R. A review of energy harvesting using piezoelectric materials: State-of-the-art a decade later (2008–2018). *Smart Mater. Struct.* **2019**, *28*, 113001. [CrossRef]
3. Ferdous, R.M.; Reza, A.W.; Siddiqui, M.F. Renewable energy harvesting for wireless sensors using passive RFID tag technology: A review. *Renew. Sustain. Energy Rev.* **2016**, *58*, 1114–1128. [CrossRef]
4. Gao, M.Y.; Wang, P.; Cao, Y.; Chen, R.; Liu, C. A rail-borne piezoelectric transducer for energy harvesting of railway vibration. *J. Vibroeng.* **2016**, *18*, 4647–4663. [CrossRef]
5. Erturk, A.; Inman, D.J. On mechanical modeling of cantilevered piezoelectric vibration energy harvesters. *J. Intell. Mater. Syst. Struct.* **2008**, *19*, 1311–1325. [CrossRef]
6. Zhang, Y.; Nakano, K.; Zheng, R.; Cartmell, M.P. Adjustable nonlinear mechanism system for wideband energy harvesting in rotational circumstances. *J. Phys. Conf. Ser.* **2016**, *744*, 12079. [CrossRef]
7. Gu, L.; Livermore, C. Passive self-tuning energy harvester for extracting energy from rotational motion. *Appl. Phys. Lett.* **2010**, *8*, 081904. [CrossRef]
8. Gu, L.; Livermore, C. Compact passively self-tuning energy harvesting for rotating applications. *Smart Mater. Struct.* **2011**, *1*, 015002. [CrossRef]
9. Wang, H.; Tang, L. Modeling and experiment of bistable two-degree-of-freedom energy harvester with magnetic coupling. *Mech. Syst. Signal Process.* **2017**, *86*, 29–39. [CrossRef]
10. Zhou, S.; Yan, B.; Inman, D.J. A novel nonlinear piezoelectric energy harvesting system based on linear-element coupling: Design, modeling and dynamic analysis. *Sensors* **2018**, *18*, 1492. [CrossRef]
11. Deng, H.; Du, Y.; Wang, Z.; Ye, J.; Zhang, J.; Ma, M.; Zhong, X. Poly-stable energy harvesting based on synergetic multistable vibration. *Commun. Phys.* **2019**, *1*, 21. [CrossRef]
12. Daqaq, M.F.; Masana, R.; ErturkX, A.; Quinn, D.D. On the role of nonlinearities in vibratory energy harvesting: A critical review and discussion. *Appl. Mech. Rev.* **2014**, *66*, 040801. [CrossRef]
13. Ferrari, M.; Ferrari, V.; Guizzetti, M.; Ando, B.; Baglio, S.; Trigona, C. Improved energy harvesting from wideband vibrations by nonlinear piezoelectric converters. *Sens. Actuators A Phys.* **2010**, *162*, 425–431. [CrossRef]
14. Ferrari, M.; Bau, M.; Guizzetti, M.; Ferrari, V. A single-magnet nonlinear piezoelectric converter for enhanced energy harvesting from random vibrations. *Sens. Actuators A Phys.* **2011**, *172*, 287–292. [CrossRef]
15. Stanton, S.C.; McGehee, C.C.; Mann, B.P. Nonlinear dynamics for broadband energy harvesting: Investigation of a bistable piezoelectric inertial generator. *Phys. D* **2010**, *239*, 640–653. [CrossRef]
16. Stanton, S.C.; Erturk, A.; Mann, B.P.; Inman, D.J. Nonlinear piezoelectricity in electroelastic energy harvesters: Modeling and experimental identification. *J. Appl. Phys.* **2010**, *108*, 074903. [CrossRef]
17. Kim, P.; Seok, J. Dynamic and energetic characteristics of a tri-stable magnetopiezoelastic energy harvester. *Mech. Mach. Theory* **2015**, *94*, 41–63. [CrossRef]
18. Kim, P.; Son, D.; Seok, J. Triple-well potential with a uniform depth: Advantageous aspects in designing a multi-stable energy harvester. *Appl. Phys. Lett.* **2016**, *108*, 243902. [CrossRef]
19. Fang, S.; Zhou, S.; Yurchenko, D.; Yang, T.; Liao, W.-H. Multistability phenomenon in signal processing, energy harvesting, composite structures, and metamaterials: A review. *Mech. Syst. Signal Process* **2022**, *166*, 108419. [CrossRef]
20. MElhadidi; Helal, M.; Nassar, O.; Arafa, M.; Zeyada, Y. Tunable bistable devices for harvesting energy from spinning wheels. In *Active and Passive Smart Structures and Integrated Systems*; SPIE: Bellingham, WA, USA, 2015; pp. 235–247. [CrossRef]
21. Fang, S.; Fu, X.; Liao, W.H. Asymmetric plucking bistable energy harvester: Modeling and experimental validation. *J. Sound Vib.* **2019**, *459*, 114852. [CrossRef]
22. Xie, Z.; Xiong, J.; Zhang, D.; Wang, T.; Shao, Y.; Huang, W. Design and experimental investigation of a piezoelectric rotation energy harvester using bistable and frequency up-conversion mechanisms. *Appl. Sci.* **2018**, *8*, 1418. [CrossRef]
23. Zou, H.; Zhang, W.; Li, W.; Wei, K.; Gao, Q.; Peng, Z.; Meng, G. Design and experimental investigation of a magnetically coupled vibration energy harvester using two inverted piezoelectric cantilever beams for rotational motion. *Energy Convers. Manag.* **2017**, *148*, 1391–1398. [CrossRef]
24. Tan, Q.; Fan, K.; Guo, J.; Wen, T.; Gao, L.; Zhou, S. A cantilever-driven rotor forefficient vibration energy harvesting. *Energy* **2021**, *235*, 121326. [CrossRef]
25. Wang, Z.; He, L.; Gu, X.; Yang, S.; Wang, S.; Wang, P.; Cheng, G. Rotational energyharvesting systems using piezoelectric materials: A review. *Rev. Sci. Instrum.* **2021**, *92*, 041501. [CrossRef] [PubMed]
26. Khameneifar, F.; Moallem, M.; Arzanpour, S. Modeling and analysis of a piezoelectric energy scavenger for rotary motion applications. *J. Vib. Acoust.* **2011**, *133*, 011005. [CrossRef]
27. Khameneifar, F.; Arzanpour, S.; Moallem, M. A piezoelectric energy harvester for rotary motion applications: Design and experiments. *IEEE/ASME Trans. Mechatron.* **2013**, *18*, 1527–1534. [CrossRef]
28. Guan, M.; Liao, W.H. Design and analysis of a piezoelectric energy harvester for rotational motion system. *Energy Convers. Manag.* **2016**, *111*, 239–244. [CrossRef]

29. Zhang, Y.; Zheng, R.; Kaizuka, T.; Su, D.; Nakano, K. Study on tire-attached energy harvester for low-speed actual vehicle driving. *J. Phys. Conf. Ser.* **2015**, *660*, 012126. [CrossRef]
30. Fu, H.; Yeatman, E.M. A methodology for low-speed broadband rotational energy harvesting using piezoelectric transduction and frequency up-conversion. *Energy* **2017**, *125*, 152–161. [CrossRef]
31. Machado, S.P.; Febbo, M.; Ramírez, J.M.; Gatti, C.D. Rotational double-beam piezoelectric energy harvester impacting against a stop. *J. Sound Vib.* **2020**, *469*, 115141. [CrossRef]
32. Mei, X.T.; Zhou, S.X.; Yang, Z.C.; Kaizuka, T.; Nakano, K. A tri-stable energy harvester in rotational motion: Modeling, theoretical analyses and experiments. *J. Sound Vib.* **2019**, *469*, 115142. [CrossRef]
33. Zhang, Y.; Zheng, R.; Nakano, K.; Cartmell, M.P. Stabilising high energy orbit oscillations by the utilisation of centrifugal effects for rotating-tyre-induced energy harvesting. *Appl. Phys. Lett.* **2018**, *112*, 143901. [CrossRef]
34. Mei, X.T.; Zhou, S.X.; Yang, Z.C.; Kaizuka, T.; Nakano, K. Enhancing energy harvesting in low-frequency rotational motion by a quad-stable energy harvester with time-varying potential wells. *Mech. Syst. Signal Process.* **2021**, *148*, 107167. [CrossRef]
35. Ma, X.; Li, H.; Zhou, S.; Yang, Z.; Litak, G. Characterizing nonlinear characteristics of asymmetric tristable energy harvesters. *Mech. Syst. Signal Process.* **2022**, *168*, 108612. [CrossRef]
36. Man, D.; Zhang, Y.; Xu, G.; Kuang, X.; Xu, H.; Tang, L.; Han, T. Improving energy harvesting from low-frequency excitations by a hybrid tri-stable piezoelectric energy harvester. *Alex. Eng. J.* **2023**, *76*, 153–165. [CrossRef]